

ORIGINAL ARTICLE

Investigating diverse photogrammetric techniques in the hazard assessment of historical sites of the Museum of the Coal Basin Area in Będzin, Poland

Ewa Świerczyńska ¹, Krzysztof Karsznia ^{1*}, Krzysztof Książek ¹ and Waldemar Odziemczyk ¹

¹Faculty of Geodesy and Cartography, Warsaw University of Technology, Pl. Politechniki 1, 00-661, Warsaw, Poland

*krzysztof.karsznia@pw.edu.pl

Abstract

Assessing the condition of historical sites at risk requires an interdisciplinary approach based on combining multiple measurement technologies. Due to the dynamic development of technology, non-invasive remote sensing methods are gaining significant importance. Among these techniques is photogrammetry based on images taken from unmanned aerial vehicles (UAVs) and those taken with a smartphone. In the study, the authors specified the possibilities and limitations of using remote photogrammetric methods to build accurate digital models of the walls of historic buildings with cracks in them. Point clouds, TIN grids, and façade orthophotos were examined. Statistical analysis was used to determine the repeatability of the data. Two parameters were identified that affect the accuracy of the data: the first – the direction of the segment between two points in the façade plane, and the second – the distance of the segment between two points in the plane of the façade. The study showed that the average accuracy of crack width measurements on the data acquired with the DJI Mavic 3 Enterprise RTK is 1 mm. Testing of crack width measurements using a Samsung Galaxy S20 FE smartphone showed an average absolute error of 0.24 mm. Based on the results, it was concluded that the images acquired using mobile devices can be used to determine changes in crack widths on walls.

Key words: historical objects, 3D models, cracks, point cloud, smartphone, TLS

1 Introduction

Developing modern geoinformation technologies, including survey instruments and methods, opens many interdisciplinary opportunities for quantity surveying. One of the main development trends is risk management (Jigyasu, 2005). This issue concerns using geodetic knowledge in effective risk management, structural monitoring, and assessing and identifying phenomena. The literature also gives many examples of the application of surveying systems in studying the condition of historical objects. For example, in the publication by Bolognesi et al. (2014), the authors considered various strategies for processing photogrammetric data acquired during the inventory of a historical 15th-century castle. The measurements were verified against analogous point clouds obtained using terrestrial

laser scanning. The obtained accuracy at the level of 1 cm enables executing precise inventory works for cultural heritage purposes.

Generally, geodetic monitoring of historical sites utilizes various technologies and inventory methods. They can be divided into invasive (or tactile), i.e., those that interfere with the structure of the measured objects, and non-invasive (or contactless), i.e., not requiring such interference (Woźniak, 2009). Among the former, we can distinguish all kinds of inclinometers (Ornoch et al., 2021) or crackmeters (Woźniak and Woźniak, 2020), as well as the geometric levelling method, enabling the precise study of vertical changes (Baselga et al., 2011). Classical tachymetric inventory is also used (Karsznia, 2023). Another interesting approach is the application of angular intersections described in Baselga et al. (2011). These methods are exact, but mounting sensors or surveying points on

historical structures requires permission from the conservation officer. Hence, the only acceptable methods for obtaining repeatable readings are solutions based on photogrammetry and remote sensing (Di Stefano et al., 2020; Markiewicz et al., 2019). A solution may be laser scanning technology utilizing a spatial polar coordinate system (Buill et al., 2020; Woźniak et al., 2015). In this way, information about the object's shape is obtained based on the point cloud, a spatial and quasi-continuous representation of the surveyed surface.

Based on capturing multisource data, a monitoring system was developed for the objects of the Coal Basin Area Museum in Będzin (Karsznia, 2024). Due to their historical importance, the objects cannot be subjected to invasive techniques (mounting signs and measuring apparatus directly on the surveyed structures). Integrating diverse data resulting from survey campaigns with highly precise, real-time inclinometer time series enables composing a coherent risk-management system, empowering a dedicated knowledge base used for further modelling.

Tachymetric measurement using a total station is a frequently used method for studying the deformation of difficult-to-access objects (Gairns, 2008; Shevchenko et al., 2020). The total station method can be used as a standalone or complement to other methods that allow more detailed imaging, like photogrammetry or laser scanning (Baca et al., 2015).

Problems of accessibility to the ever-emerging signs of structural damage (gaps and expansion joints) determine the need to use small and fully mobile measurement technologies (Świerczyńska et al., 2023).

Unmanned aerial vehicles and smartphones can record measured objects with a mounted or built-in laser scanner. Then, the coordinates of the points in the spatial coordinate system are acquired directly with the sensor (Lohani and Ghosh, 2017). These devices can also capture images of the measured object using a mounted or built-in digital camera. Then, the coordinates of points in the spatial coordinate system are acquired from photogrammetric processing of the images using appropriate software. Most image-based 3D reconstruction software has its own algorithm for generating a dense point cloud (Murtiyoso and Grussenmeyer, 2017).

Inexpensive scanning devices such as the iPhone 13 Pro LiDAR (Light Detection and Ranging) have recently become standard. LiDAR technology is often implemented in UAVs and relies on measuring the timing of the return pulse emitted from a laser transmitter to a laser receiver (Lohani and Ghosh, 2017). On the other hand, over the past few years, studies have been conducted to determine the suitability of LiDAR technology in the iPhone for the inventory of architectural details (Teppati Losè et al., 2022) or small rooms (Zaczek-Peplinska, 2023). Studies on crack detection have shown that with high resolution, short iPhone distance, and using additional tie points, it is possible to measure very small cracks (even about 1 mm) (Błaszczak-Bąk et al., 2023). A comparison of the iPad's LiDAR sensor, a handheld laser scanner, and traditional forest inventory equipment shows a high detection rate of tree trunks over 10 cm in diameter (Gollob et al., 2021).

Thanks to the development of technology and the placement of cameras with increasingly better smartphone performance, data similar to that obtained with the iPhone can be obtained with any smartphone. The difference lies in the indirect way of obtaining them rather than the direct way. The accuracy and resolution of the output data depend on a number of factors: the quality and number of images taken, the algorithm, and the image processing parameters (Fawzy, 2019). Using short-range photogrammetry with ground-based equipment, it is possible to record an area even of considerable size (for example, 25 × 55 m) with high resolution (for example, 1 mm) (Sapirstein, 2016). Short-range photogrammetry technology produces results similar to those of laser scanning technology (in the form of point clouds). However, it differs from laser scanning in the process of acquiring and processing input data (Baltavias, 1999). The research shows that the standard de-

viation for point clouds, obtained by processing images acquired with different cameras, compared to terrestrial laser scanning, is about 5 cm (Jaud et al., 2019). However, the integration of a digital camera with sensors such as an accelerometer, magnetometer, gyroscope and GNSS antenna in a mobile device gives users the ability to map surface changes of objects with a repeatability of about 4 mm (Corradetti et al., 2021). These solutions inspired the authors to undertake a comprehensive study of the technical condition of historic buildings located in endangered (post-mining) areas. The field and analytical work has been carried out within the framework of two consecutive scientific projects granted by the Council of Scientific Disciplines of Civil Engineering, Geodesy, and Transportation. The test sites belong to the Museum of the Coal Basin Area in Będzin, Silesian Voivodeship, Poland, with which Warsaw University of Technology collaborates in the field of risk management and assessing the condition of historic objects.

The aim of this work was to assess the accuracy of two types of data (from the UAV and a smartphone) that will feed a unified facility monitoring system for the entire Mieroszewski Palace. The research attempts to determine the feasibility of using technology based on photogrammetric image processing to assess the technical condition of object surfaces. The innovative nature of the research consisted in acquiring working photogrammetric data in such a way that it was possible to detect changes in the dimensions of the cracks. These changes were assumed to be about 1 mm.

The paper is organized as follows. In section 2, the research objects with their structural problems are presented. Section 3 presents the methodology of the research conducted and the theoretical aspects of the statistical analyses. In section 4, we present the specification of the equipment used in the study and the characteristics of the data obtained. In section 5, the results of the research are described. This section is divided into two subsections: the ability to assess the technical condition of objects based on UAV data and the ability to assess the technical condition of objects based on smartphone data. In section 6, we compare the obtained results with existing studies using similar technologies. In section 7, a summary and concluding remarks are presented.

2 Research sites

The research was carried out on historical sites of the Museum of the Coal Basin Area in Będzin, including Mieroszewski Palace, Będzin Castle, Będzin Underground, and the synagogue "Mizrachi". For practical reasons, our research was limited to the results obtained at the Mieroszewski Palace.

The Mieroszewski Palace was built in 1702 and was a typical 18th-century noble French-style residence (Figure 1). It is a one-story palace with a double-arched mansard roof and an amphitheatre-like arrangement of rooms. Rich polychrome paintings dated to the 18th century are on the interior walls. On the eastern side, a wide driveway leads to the main entrance. In addition, on the west side, there is a park with stone sculptures and interesting tree specimens. The whole forms an architectural layout, reflecting an 18th-century park and palace composition (Museum of the Coal Basin, 2024).

Based on data from the Polish Geological Institute, it can be concluded that the city of Będzin is strongly influenced by the impact of the mining industry (PGI, 2024). Figure 2 shows the range of the surrounding mining areas. They are located in a radius of about 2.5 kilometres. However, the space covered by the predicted harmful effects of the mining works is in the immediate vicinity. This neighbourhood means that such factors can be responsible for potential damage to the Museum facilities.

The main reason for the degradation of the subsoil of Castle Hill and its surroundings (including the area of the Mieroszewski Palace) can be traced to the Będzin Fault, which cuts through the northeastern part of the city. GPR and gravity surveys have shown



Figure 1. The Mieroszewski Palace in Będzin – 1702

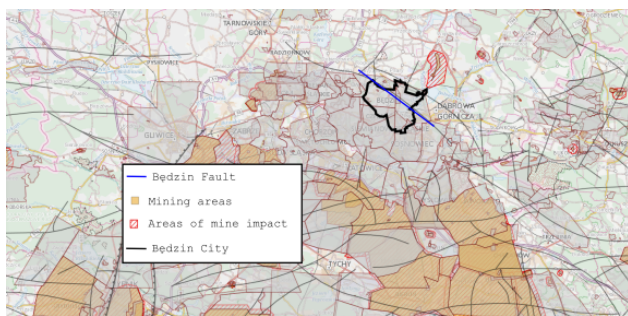


Figure 2. Location of the city of Będzin in relation to the mining areas (PGI, 2024)

that mining activities have caused rock mass movements. The activation of the Będzin Fault can be seen in the cracks of buildings located in the Castle Hill area. The movement of the tectonic structure is compounded by the geology of the area and the impermanent casing of the Będzin Underground (Figure 3), which is currently an unfinished German air raid shelter. Its course crosses the castle hill, significantly affected by the geological activity of the Będzin Fault (Stec, 2007).

Figure 4 shows the area with the highest probability of ground destruction resulting from the Będzin Fault. It extends to the north-eastern walls of the castle.

Among other factors impacting the technical condition of the monitored sites may be climatic and environmental changes like air pollution or acid rains (Chen et al., 2013; Xie et al., 2004), as well as the proximity of monuments to major transportation routes, the expansion of the road network, or renovation works carried out.

As a result of the above factors, the technical condition of the Mieroszewski Palace included in the survey is deteriorating. Cracks and fissures have appeared on the palace walls, requiring monitoring. The most significant changes are noticeable along the walls connecting the central part of the building with the annexed part on the southern side. Cracks are also present on the ceiling, located above the palace's second floor.

3 Research methodology

The presented studies encompass non-invasive mobile technologies limited to unmanned aerial vehicles (UAVs) for the exterior parts and the smartphones used in the interior. Additionally, total station survey data was used to boost the accuracy in generating photogrammetric point clouds.

The methodology of data acquisition, processing, and elab-



Figure 3. Będzin Underground – view of the Będzin Fault zone



Figure 4. Location of sites to be monitored in relation to the Będzin Fault

oration is presented in Figure 5. The exterior façade of the Mieroszewski Palace and the fortified castle were recorded in cooperation with NaviGate Ltd. using the DJI Mavic 3 Enterprise RTK flying system. It is equipped with a telephoto camera with a 1/2-inch CMOS sensor with an effective resolution of 12 MP (maximum image size: 4000 x 3000), a field of view of 15°, an aperture of f/4.4 and a format equivalent to 162 mm (Pix4D, 2023).

During the survey, the interior walls of the palace were recorded using the Pix4Dcatch application installed on a Samsung Galaxy S20 FE smartphone. It allows acquiring images from which a point cloud representing the measured objects is generated in the Pix4Dcloud software.

Figure 6 shows photographs of the experimental and internal measurements taken at the Mieroszewski Palace. Figure 6a shows a DJI Mavic 3 Enterprise RTK in a flight, and Figure 6b shows an inventory of the attic floor using a Samsung Galaxy S20 FE smartphone.

During fieldwork, tie and reference points were established. Reference points were marked on objects surrounding the palace, and tie points were marked on the palace façade. Retroreflective tape targets were used for both groups of points. The function of these points was twofold. Firstly, they constitute a matrix for photogrammetric studies, counteracting the phenomenon of error accumulation. Secondly, a group of points located on two sides of the crack visible on the outer wall of the building were measured. Cyclic surveying of these points provides information about changes occurring in the crack area independent of photogrammetric studies.

All points were measured from two stations (A and B) stabilized only for the duration of a given measurement, which is an advantage given the historic nature of the area, i.e., the garden adjacent to the Palace. The locations of the tie points and the two survey

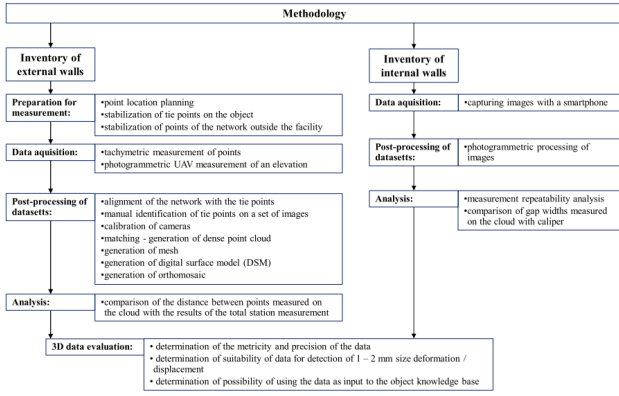


Figure 5. The main stages of the proposed measurement methodology

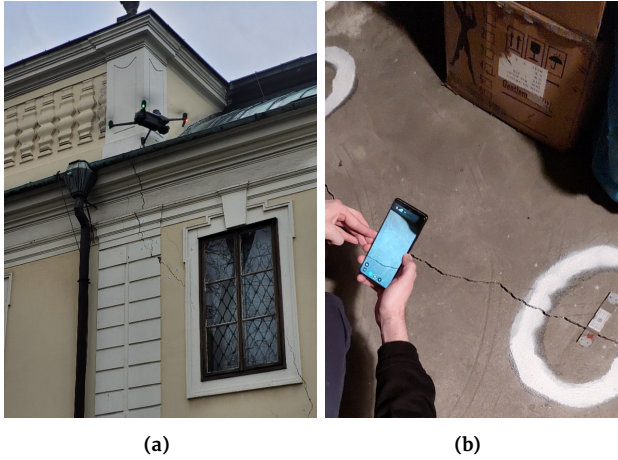


Figure 6. Object inventory by two methods: (a) – using UAV by DJI Mavic 3 Enterprise RTK; (b) – using Samsung Galaxy S20 FE smartphone

positions are shown in Figure 7. The marked points were measured using a Leica TS 09 total station. Since the locations were not referenced to an external coordinate system, each has a separate local system. For further analysis, it was necessary to convert the XYZ coordinates obtained from the measurements to a common system. This system was defined so that one of the axes of the coordinate system (Y) was parallel to the façade of the building. The orientation of the local coordinate system axes is shown in Figure 8. The Z-axis was assumed to be vertical. Assuming the coordinate system in this way facilitated the data analysis presented later in the article. The horizontal coordinates (X, Y) and Z vertical coordinate were calculated separately. The object's extent (excluding reference points) does not exceed 50 m. For such a distance, the effect of the Earth's curvature does not exceed 0.2 mm, the vertical line convergence is $5''$, and the linear effect of this convergence for a building height of 12 m is below 0.1 mm. Considering the measurement precision (limited by the target marking type) of about 1 mm, the ortho-cartesian coordinate system can be assumed for further analyses.

This step was followed by averaging the coordinates obtained from the two measurement stations. To do this, a coordinate transformation was performed according to Equation (1). This conversion was a four-parameter transformation of the 2D+1 type, consisting of a rotation around the vertical axis by an angle α and a 3D shift, as follows:

$$P_{sec.} = \begin{bmatrix} \cos \alpha & \sin \alpha & 0 \\ -\sin \alpha & \cos \alpha & 0 \\ 0 & 0 & 1 \end{bmatrix} \cdot P_{prim.} + T_0 \quad (1)$$



Figure 7. Total station measurement from two stands to the tie points located on the front facade of the Mioszowski Palace, reference points on objects surrounding the palace, and the control points mounted along the main crack

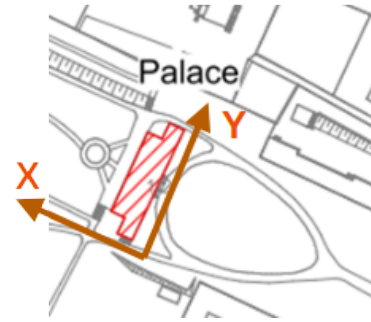


Figure 8. The local coordinate system of the Mioszowski Palace

where:

- $P_{sec.}$ – coordinate of points in a secondary coordinate system,
- $P_{prim.}$ – coordinate of points in a primary coordinate system,
- α – angle of rotation in the horizontal plane,
- T_0 – 3D shift vector.

The reference points (101, 102, 103, 104, and 107), located outside the site, were used to determine the transformation parameters (angle α and vector T_0). The sets of coordinates for sites A and B were then averaged, and transformed to a common system. The coordinates thus obtained were taken as final for further analysis.

Table 1 shows the accuracies of the tie points and reference points obtained from total-station measurement and adjusted, respectively. These are the differences between the coordinates of the points deployed on the Palace façade (1 – 21) and the surrounding objects (101 – 104, 107) captured from standpoints A and B.

In the final alignment, the alignment of the total station over a fixed reference point was not considered. The coordinates of stations A and B were determined from reference points (101 – 104, 107), located on the structures adjacent to the palace. In this case, the coordinates of these stations were determined in the same way as the coordinates from the free stations.

Two types of error can determine the precision of the acquired data:

- absolute error, which describes the accuracy of a single measurement, is the difference between the measured value and the actual value:

$$\varepsilon(x) = |x - x_0| \quad (2)$$

- relative error, which describes the accuracy of a measurement with an instrument, is the ratio of the difference between the mea-

Table 1. Differences between the coordinates of points on the Palace façade (tie points) and the surrounding objects (reference points) captured from stations A and B (after transformation)

Point number	Accuracy				Point number	Accuracy			
	dX [mm]	dY [mm]	dH [mm]	dP [mm]		dX [mm]	dY [mm]	dH [mm]	dP [mm]
1	-1,0	-0,4	0,5	1,2	15	-0,1	-1,0	-0,2	1,0
2	-0,3	0,3	-1,6	1,7	16	-0,1	-1,1	0,1	1,1
3	-1,0	0,8	-0,5	1,4	17	-0,3	-1,0	-1,1	1,5
4	-1,9	0,0	-1,4	2,4	18	-1,4	-1,7	0,6	2,3
5	-1,1	-1,6	0,3	2,0	19	-1,6	-0,8	-1,8	2,5
6	-1,0	0,4	-0,5	1,2	20	-2,1	-0,5	-1,8	2,8
7	-1,5	-0,9	-0,4	1,8	21	-1,4	-1,1	0,9	2,0
8	-7,5	-4,5	-0,7	8,8	101	1,5	0,3	-0,9	1,8
9	-1,1	-1,8	0,6	2,2	102	-0,2	0,5	-0,1	0,5
10	-1,1	0,0	-1,0	1,5	103	-1,8	0,9	-0,7	2,1
11	-0,3	-1,2	0,1	1,2	104	-0,2	-0,1	0,5	0,5
12	-1,4	-2,5	-0,6	2,9	105	-0,3	0,7	-0,9	1,2
13	-0,2	-2,3	-1,3	2,6	106	1,8	-0,5	0,4	1,9
14	-0,9	-3,1	-0,8	3,3	107	-1,0	-1,8	0,2	2,1

sured value and the actual value to the measured value:

$$\delta(x) = \frac{|x - x_0|}{x} \cdot 100\% \quad (3)$$

where x is the measured value, and x_0 is the real value.

The accuracy of the point clouds resulting from photogrammetric processing depends on several factors, including the size of the registered object, the distribution of tie points, or the number of images used in the alignment process. A correlation coefficient is calculated to test the correlation between two variables, for example, X and Y . Obviously, the two sets of variables should have the same number of observations in a scalar form. It is worth noting that the correlation coefficient only determines the degree of linear dependence of two variables (Press et al., 1992). The Pearson correlation coefficient is calculated from the following formula (Pearson, 1896):

$$\rho(X, Y) = \frac{1}{N-1} \sum_{i=1}^N \left(\frac{X_i - \bar{X}}{\sigma_X} \right) \left(\frac{Y_i - \bar{Y}}{\sigma_Y} \right) \quad (4)$$

where:

- X and Y – first and second set,
- N – the number of both sets,
- \bar{X} and \bar{Y} – the mean of X and the mean of Y ,
- σ_X and σ_Y – the standard deviation of X and the standard deviation of Y .

The point clouds obtained from the research were analyzed for their metricity, mainly in the plane coinciding with the wall of the front façade of the palace.

4 Data specification

As a result of the measurement and processing of the obtained results, a very high accuracy of the position of the signs on the front façade was obtained. The average error in the position of the adjustment points in the local coordinate system does not exceed 1 mm. This accuracy further allowed the generation of a “true ortho” façade with equally high accuracy, i.e. the degree of agreement between the model parameters and the actual quantities. This demonstrates the high accuracy of the spatial data.

As a result of data registration and processing, point clouds and spatial models of the Będzin Palace were obtained. Figure 9a shows point clouds which are quasi-continuous geometric representations of the palace. They were created due to processing several hundred images with specialized photogrammetric software using the image-matching method.

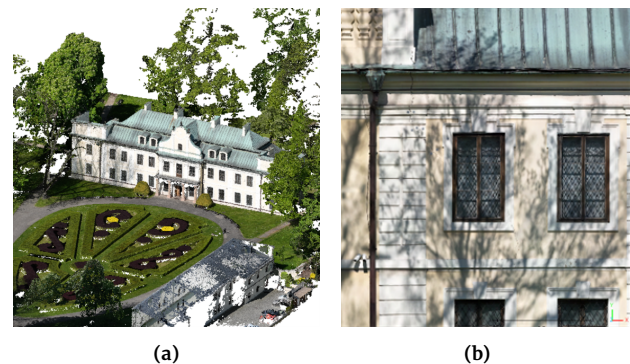


Figure 9. Views of models representing the Mieroszewski Palace: (a) – perspective view; (b) – part of the palace façade with the location of the largest crack marked

It should be noted that the degree of detail of the generated spatial data is relatively high. The density of the point cloud representing the palace is 300 points/m². This parameter is a property that characterizes this data, as it determines the ability to recognize individual objects and identify details. Based on the density, the average distance between neighbouring points of the cloud is determined. In the process of automatic image matching, a discretization of the object in the form of nodal points of a regular grid of squares is carried out. Assumption that the average distance between the points of the cloud representing the palace is 6 cm may help imagine the spatial precision of the data. The space between the cloud points is filled at the stage of modeling and applying the texture to the triangle grid.

The data presented in Figure 9a are the results of the processed images, taken using an unmanned aerial system during a horizontal flight. In addition to the horizontal missions, a vertical flight was carried out along the front façade of the Mieroszewski Palace. The images obtained from this flight were used to analyze the technical condition of the façade. Processing about 1000 photos with specialized photogrammetric software using the image matching method, resulted in a point cloud with a density of 62500 points/m². It gives an average distance between neighbouring points of the cloud of about 4 mm. In addition, the vertical flight images created a “true ortho” of the front façade of the Mieroszewski Palace. Its fragment is presented in Figure 9b.

A true orthophoto of the wall is the analogue of a true orthophoto of the terrain. These two orthophotos differ in the plane on which the image is projected. In “true ortho”, the wall is a vertical plane, not a horizontal plane as in the case of terrain. The most crucial

geometric property remains unchanged: the elimination of radial displacement of objects projecting above the wall (such as ornaments, balustrades, or columns) or “blind spots”, understood as areas obscured by leaning projecting objects. This means that objects lying on the vertical plane, which approximates the wall surface, as well as those projecting above it, are depicted in orthogonal projection. Specialized photogrammetric software such as Pix4Dmatic or Pix4Dmapper is used to eliminate radial displacements.

The precision of “true ortho” is defined by the field pixel size. This is the actual distance to which the smallest uniform element of a digital image corresponds. As a result of the conducted research, a “true ortho” of the front façade of the Mioszowski Palace was obtained with a field pixel size of 0.7 mm. The order of this size indicates a very high degree of detail and recognition of individual details.

In addition to the high level of detail, the “true ortho” façade is also characterized by a high degree of accuracy, achieved by adjustment points evenly distributed on the front wall of the palace. Figure 10 shows the distribution of the accuracy of the position of the adjustment points evenly distributed on the front wall of the Mioszowski Palace. Their average errors along the length and height of the façade are presented on a colour scale.

Average tie points errors were determined based on the modified Formula (5) in the following general version:

$$\Delta(x_i) = \left| \left(x_i^{tach.} - x_i^{ortho} \right) - \frac{\sum_{j=1}^n (x_j^{tach.} - x_j^{ortho})}{n} \right| \quad (5)$$

$$\Delta(y_i) = \left| \left(y_i^{tach.} - y_i^{ortho} \right) - \frac{\sum_{j=1}^n (y_j^{tach.} - y_j^{ortho})}{n} \right|$$

where:

$x_i^{tach.}, y_i^{tach.}$ – tie points coordinates calculated from tacheometry measurements,
 x_i^{ortho}, y_i^{ortho} – tie points coordinates measured at “true ortho” façade.

The modification is due to the need to compare 2D and 3D data. Its application was possible because, during the adjustment of the total-station measurement, the YOY plane of the geodetic local system was adapted along the façade. For accuracy analysis, the YOY plane of the geodetic local system has been replaced by a two-dimensional XOY system, where the X axis is parallel to the façade length ($x_i^{tach.}$), and the Y axis is parallel to the façade height ($y_i^{tach.}$).

The differences are evaluated in terms of the average difference between the coordinates obtained by the two techniques because the coordinates of the tie points obtained from total-station surveys are expressed in a different local coordinates system than the tie points measured on the façade “true ortho”.

The errors of the tie points concerning the X and Y axes are equal to the deviation of the individual differences between the coordinates obtained with the two techniques from the average differences between the coordinates obtained with the two techniques. Such a procedure replaced the need to transform the “true ortho” façade coordinate system relative to the coordinate system of the total station measurement.

Since during the alignment of the total station survey, the YOY plane of the geodetic local system was taken along the façade wall, the transformation would only consist of shifting the “true ortho” coordinate system by the: $X = \frac{\sum_{j=1}^n (x_j^{tach.} - x_j^{ortho})}{n}$ and $Y = \frac{\sum_{j=1}^n (y_j^{tach.} - y_j^{ortho})}{n}$ vectors.

The average errors of the tie points range from 0 to almost 6 mm. However, the largest error value has only one point (point number 8) in a hard-to-reach place. The average error of the position of the adjustment points on the “true ortho” along the length of the façade is 1 mm, which is within the limit of the tachymetric mea-

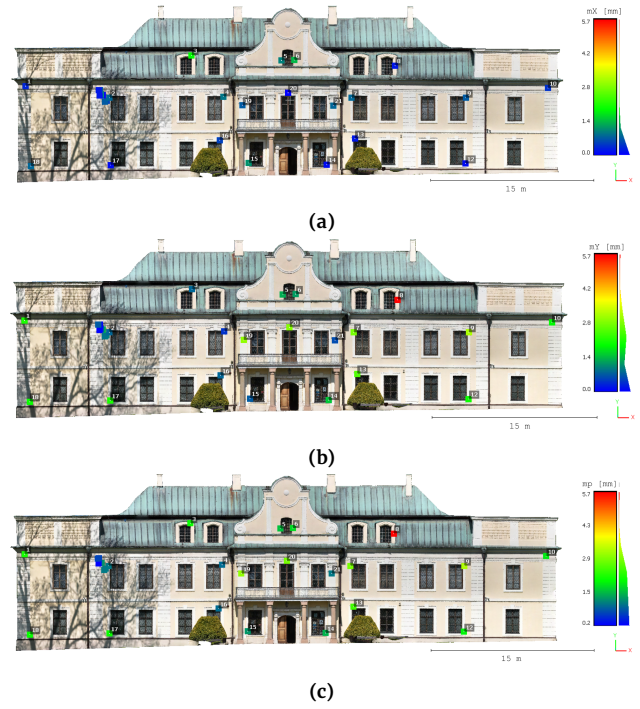


Figure 10. Analysis of the accuracy of the position of the tie points along the (a) – length of the front façade of the Mioszowski Palace; (b) – height of the front façade of the Mioszowski Palace; (c) – analysis of the accuracy of the 2D position of the tie points

surement error. In contrast, the average error of the position of the adjustment points on “true ortho” along the façade height is more than 3 mm. Thus, a decrease in accuracy in the vertical direction and high accuracy in the horizontal direction are noticeable.

5 Results

According to the scheme presented in Figure 5, the results of the measurements were analyzed separately. First, the possibility of assessing the condition of objects based on UAV data was tested. Then, the possibility of assessing the condition of objects based on smartphone data was tested.

5.1 Façade inspection possibility on the Palace using a UAV

Even though Mioszowski Palace is located 700 meters from the Będzin Fault, cracks and fissures have appeared on its walls, which require monitoring. The most significant changes are noticeable along the walls, which connect the main part of the building with the annexed part on the south side. Around this connection, cracks and fissures are also present on the ceiling of the Palace’s second floor. Figure 11a shows the largest crack on the front façade of the Palace. It is located just around the connection between the main part of the building and the annexed part on the south side.

Survey marks were stabilized around the crack, also measured during the tacheometric inventory. In Figure 11b, these points are S1, S2, S3, S4, S5, S6 and S7. In the metric analysis of the UAV-derived data, they served as façade control points. It should be noted that these points, unlike tie points, did not take part in the image calibration and matching process. Figure 11b shows the position errors of façade control points. The differences between the coordinates of façade control points determined from the tachymetric survey and those determined from the orthophoto survey are shown in colour scales. These errors were calculated based on the Formula (5) and

Table 2. Comparison of the results of measuring the crack on the outer wall of the Palace on 2D – “true ortho” and 3D – point cloud data

Measure along the line between points	Crack size on “true ortho” façade [mm]	Size of the crack on the façade cloud [mm]	Absolute error [mm]	Relative error [%]
S1 – S2	6.7	8	1.3	16.3
S3 – S4	3.2	4	0.8	20.0
S4 – S5	4.5	4	0.5	12.5
S6 – S7	5.0	4	1.0	25.0
Average			0.9	18.4

ranged from 0.2 mm to 1.3 mm.

Table 2 shows the results of measuring the crack located on the outer wall of the Palace. This is a comparison of 2D – “true ortho” and 3D – point cloud data. The width of the crack was measured at three levels along four straight lines connecting the points S1 and S2, S3 and S4, S6 and S7. The volumes measured on ‘true ortho’ with a field pixel size of 0.7 mm were taken as the reference measurement. The results obtained from the point cloud differ from the reference by an average of 18.4%. The magnitude of the absolute error is due to the high resolution of the “true ortho” and the density of the point cloud such that the distance between cloud points averages 4 mm. The density of the point cloud is, therefore, lower than the resolution of “true ortho”. In addition, the obtained results are affected by the subjectivity of identifying the crack’s edge.

The “true ortho” metric analysis was based on all possible combinations of distances between façade control points (from S1 to S7) and all possible combinations of distances between tie points (from 1 to 10 and from 12 to 21). The distances calculated from the coordinates determined from the total station measurement were taken as reference. Total station measurement is characterized by high accuracy, as shown in Table 1. For this reason, the coordinates of the points obtained from the alignment of the tachymetric observations were taken as reference. The distances between all possible combinations of two points were calculated based on them. These are x_0 in the Formulas (2) and (3). In this way, reference distances were obtained and compared with their counterparts, which were calculated from coordinates measured on the true ortho (these are x in the Formulas (2) and (3)). The differences between the reference distances and the distances tested on the true ortho were presented in the form of relative and absolute errors according to Formulas (2) and (3).

The parameters on which the accuracy depended were:

- direction of the segment between two points in the plane of the façade – where $\varphi = 0^\circ$ means vertical orientation (along the façade height), $\varphi = 90^\circ$ means horizontal orientation (along the length of the façade), while intermediate values of φ indicate oblique directions. Thus, it was possible to check the metricity of the true ortho in directions parallel to the X-axis, in directions parallel to the Y-axis and in intermediate directions. It was also possible to answer the question in which direction the metricity of the data is the lowest and in which direction it is the highest. The method of calculating the directions of segments between two points in the plane of the façade (φ) is shown graphically in Figure 12.

- the segment’s distance between two points relative to the vertical plane of the façade – in order to check whether they are scaled in the 2D data. Then, as the distance increases, the errors of the segments increase. However, the orientation of the segment in question should be considered.

The correlation between the accuracy of the lengths of all possible combinations of segments, the lengths of these segments, and the direction of these segments are shown using graphs. Figure 13 shows the dependence of the relative (Fig. 13a) and absolute (Fig. 13b) errors of the lengths of the sections between the façade control points and the direction of the section in the façade plane. Figure 14 shows the dependence of the relative (Fig. 14a) and absolute (Fig. 14b) errors of the lengths of the sections between the

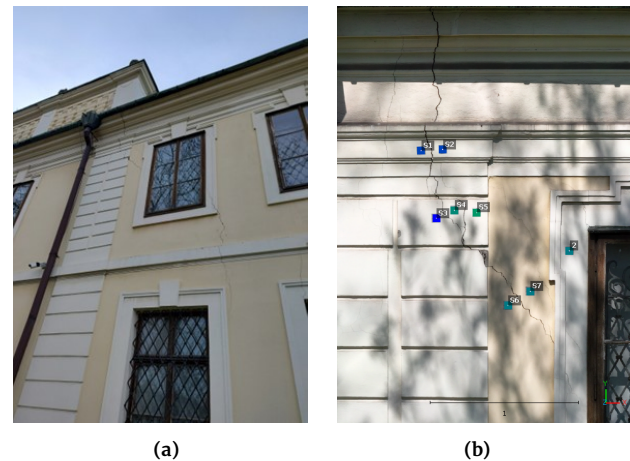


Figure 11. Effects of the inventory of cracks on the outer wall of the Mioszowski Palace: (a) – photograph of a fragment of the façade; (b) – orthophotomap made based on UAV images. The accuracy of façade control points, stabilized along the crack is shown in colour scale.

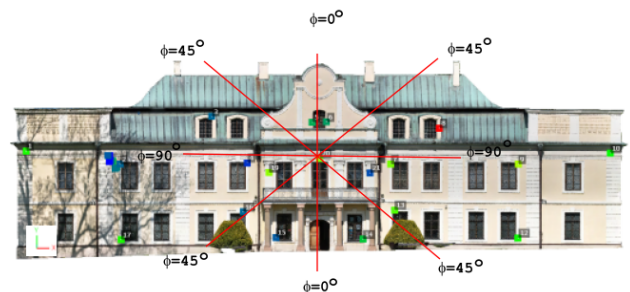


Figure 12. Method of calculating the directions of segments between two points in the plane of façade – φ

façade control points and the lengths of these sections in the façade plane. Similar graphs were generated for tie points. Figure 15 shows the dependence of the relative (Fig. 15a) and absolute (Fig. 15b) errors of the lengths of the sections between tie points and the direction of the section in the façade plane. Figure 16 shows the dependence of the relative (Fig. 16a) and absolute (Fig. 16b) errors of the lengths of the sections between tie points and the lengths of these sections in the façade plane. The point plots also include trend lines in the form of second-order polynomial functions that approximate the scatter.

Interpreting the effect of the direction of the section between two points, it should be noted that the relative errors of the sections between the façade control points are smaller for $\varphi = 0^\circ$ (vertical sections) than for $\varphi = 90^\circ$ (horizontal sections). As the direction increases, these errors increase. In contrast, the relative errors of the sections between tie points are smaller for $\varphi = 90^\circ$ (vertical sections) than for $\varphi = 0^\circ$ (horizontal sections). This fact is consistent with the geometry of the distribution of the different types of

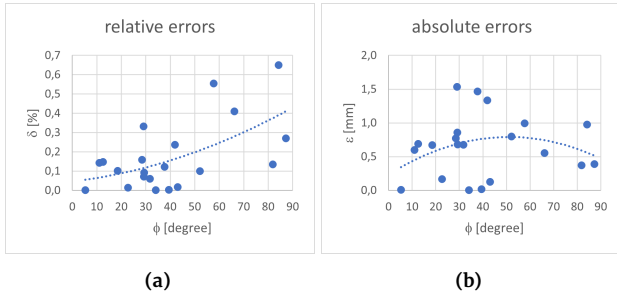


Figure 13. The dependence of section length errors between façade control points and the direction of the section in the façade plane, presented in the form of error: (a) – relative calculated from Equation (3); and (b) – absolute calculated from Equation (2) (trend lines generated using polynomials of the second order)

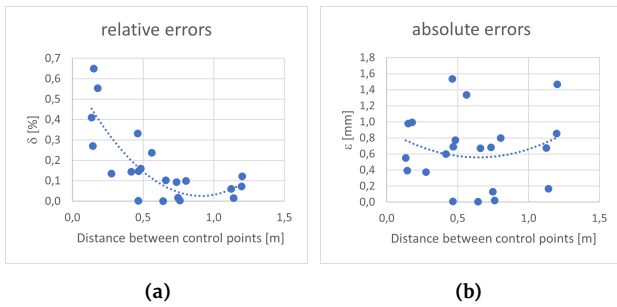


Figure 14. The dependence of section length errors between façade control points and section length in the façade plane presented in the form of error: (a) – relative calculated from Equation (3); and (b) – absolute calculated from Equation (2) (trend lines generated using polynomials of the second order)

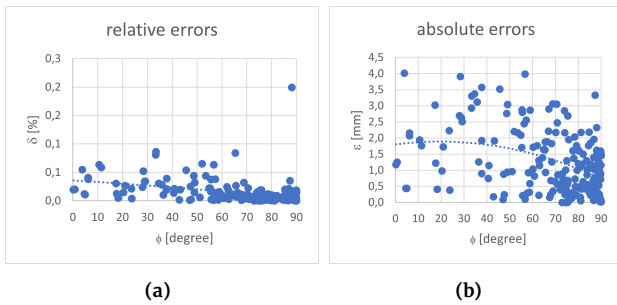


Figure 15. The dependence of segment length errors between tie points and the direction of the segment in the façade plane presented in the form of error: (a) – relative calculated from Equation (3); and (b) – absolute calculated from Equation (2) (trend lines generated using polynomials of the second order)

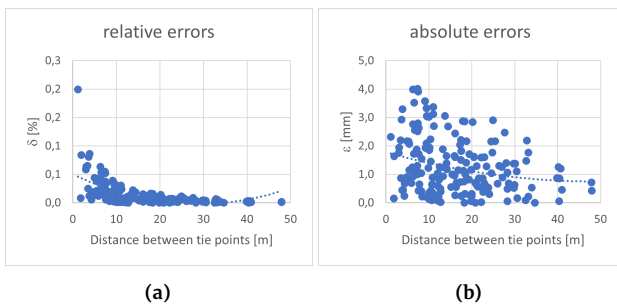


Figure 16. Dependence of section length errors between tie points and section length in the façade plane presented in the form of error: (a) – relative calculated from Equation (3); and (b) – absolute calculated from Equation (2) (trend lines generated using polynomials of the second order)

points.

In turn, the absolute errors of the sections between the façade control points are the largest for oblique directions. This is evidenced by the convexity of the trend function. In contrast, the absolute errors of sections between the tie points show a decreasing trend as the direction φ increases. These results suggest greater accuracy of linear quantities measured along the length of the wall than those measured along the height of the wall. This direction is consistent with the measurement of the width of vertical cracks on the façade.

Interpreting the effect of the segment length between two points, it should be noted that as this length increases, the relative errors of the distance between the façade control points and tie points decrease. A decreasing trend can also be observed for the absolute errors of the distance between the tie points. On the other hand, in the case of absolute errors of distance between the façade control points, there is a large dispersion of points.

Correlations between segment errors and the analyzed parameters are shown in Table 3. They were calculated according to the Formula (4) separately for the direction of segments between points and the distance of segments between points relative to the vertical façade plane.

The correlation coefficients for relative errors, whose absolute value ranges from 0.38 to 0.66, testify to the dependence of the two data sets at an average level. The values of all coefficients in Table 3 differ from the value of 0, so correlation exists. The highest correlation was observed for relative errors and distance between points. The greater the distance, the smaller the relative error, which may indicate that the calculations are correct. On the other hand, the correlation for absolute errors and direction for the control points has an increasing trend, and for the tie points it has a decreasing trend.

The correlation coefficients for absolute errors, whose absolute value ranges from 0.03 to 0.37, testify to the dependence of the two data sets at a very low level. The correlation between absolute errors of distance between combinations of tie points and analyzed parameters occurs at a higher level than the correlation between absolute errors of distance between combinations of control points and analyzed parameters. It should be noted that the correlation coefficient for the absolute error and the direction of the section is -0.37 . This is relatively high and shows that the errors of sections with directions parallel to the X-axis are relatively smaller than those with directions parallel to the Y-axis. The correlation coefficient should be considered to indicate the degree of linear dependence between two sets. It is not possible to characterize an exponential or polynomial trend with this coefficient.

5.2 Façade inspection possibility on the Palace using a smartphone

The Pix4Dcatch app installed on a Samsung Galaxy S20 FE smartphone recorded cracks on the palace's interior walls. Changes on all levels of the building, on walls and ceilings, were inventoried. Images of all cracks were processed using Pix4Dcloud software, obtaining a point cloud and TIN (Triangulated Irregular Network) model for each object.

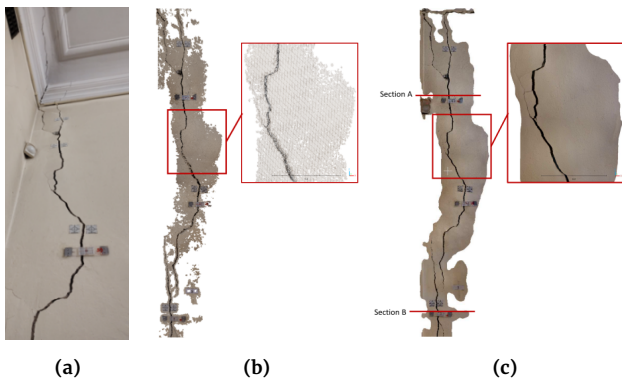
Figure 17 shows all the resultant products, such as cracks. Figure 17b shows the point cloud that represents the crack. It was generated using the Pix4Dcloud app based on images acquired using the Pix4Dcatch app installed on a smartphone. The cloud in Figure 17b has a 100 points/cm² density. This shows that the distance between cloud points is about 1 mm. In turn, Figure 17c presents the TIN model which is a triangle mesh formed from the point cloud and the texture of the images. Measuring with a precision of more than 0.5 mm on the TIN grid is possible. Such a high density of the point cloud and the resolution of the TIN model is due to the short distance between the registered object and the camera.

Table 3. Correlation coefficients between data sets

Type of points	Parameter	relative errors δ	absolute errors ε
Correlations coefficients of error distances between points S1 – S7	ϕ	0.59	0.07
	Distance between tie points	-0.66	0.03
Correlations coefficients of error distances between points 1 – 10 and 12 – 21	ϕ	-0.38	-0.37
	Distance between tie points	-0.48	-0.25

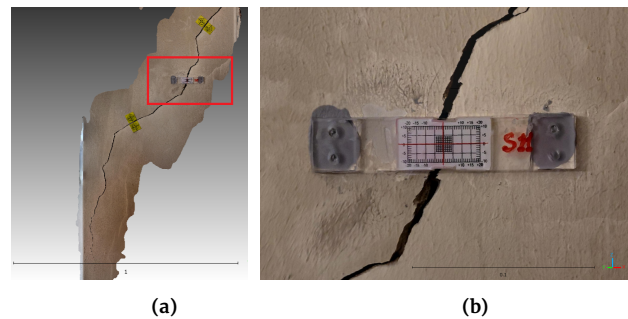
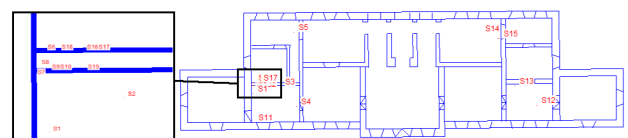
Table 4. Comparison of the results of measuring the crack on the interior wall of the Palace by two methods: the first, using a calliper, and the second, on a cloud of points with a cloud density of 100 points/cm², i.e. the point-to-point distance was about 1 mm

Measurement location	The size of the crack measured:		Absolute error [mm]	Relative error [%]
	using a caliper [mm]	on the TIN model [mm]		
Section A	6.64	6.5	0.14	2.15
Section B	7.84	7.5	0.34	4.53
Average			0.24	3.34

**Figure 17.** The results of the inventory of the cracks on the inner walls of the Mioszowski Palace: (a) – a photograph of the crack; (b) – a point cloud representing the crack, generated using the Pix4Dcloud application based on images acquired with the Pix4Dcatch application installed on a smartphone; (c) – a TIN model of the crack, generated using mobile technology with a smartphone

In the Pix4Dcatch software specification, the authors state that its accuracy is a few centimetres, while its repeatability is a few millimetres. These quantities are not very high. The described studies showed that the photogrammetric processing of images acquired with a smartphone could be sufficiently accurate and useful for the described applications.

As is known, the calibration of images without the use of tie points results in the fact that the 3D model generated in post-processing is burdened with a scale factor. This coefficient is different in each direction. The user has no control over the metric properties of the resulting model. On the other hand, however, the distortion of a 3D model, TIN mesh or point cloud is smaller the smaller the object. This property is helpful for the model of cracks on the interior walls of the palace. Admittedly, 3D models generated by photogrammetric processing of images without tie points are burdened by a scale factor. However, as Table 4 shows, the error in measuring the width of cracks is, on average, 0.24 mm or 3.34%. Measuring the length of the entire crack on a smartphone model is not as accurate, but the measured size is also larger. The accuracy of the crack width measurement may be sufficient to detect any future changes of 0.5 mm. The repeatability of the results presented in Table 4 was confirmed by repeated registration of the crack and repeated measurement of the crack width.

**Figure 18.** TIN model of one of the cracks on the wall of the palace, generated using the Pix4Dcloud application based on images acquired with the smartphone Pix4Dcatch app (a) (the red rectangle shows the location of the crackmeter); (b) close-up of the scale drawn on the crackmeter**Figure 19.** Location of crackmeters on the plan of the outline and interior walls of the Mioszowski Palace

Accurate identification of crack edges is difficult. Manual pointing of points to measure crack width is subjective. Therefore, the feasibility of using mobile technology to determine the condition of walls was assessed by measuring the graduations of crackmeters. An example of such a sensor is shown in Figure 18a. The method of attaching the device to the wall surface is shown in Figure 18b.

As shown in Figure 19, the crackmeters network was stabilized on the interior walls of the Mioszowski Palace. Usually, crackmeters are used to determine changes in crack width by taking periodic readings. In the study, which aimed to determine the metricity of smartphone-acquired TIN models, they served as a base with specific dimensions. As can be seen in the figure, the graduation of the slit gauge has two main axes: horizontal and vertical. The nominal length of the horizontal axis is 4.00 cm because the horizontal scale ranges from -2.00 cm to 2.00 cm. The nominal length of the vertical axis is 2.00 cm because the vertical scale ranges from -1.00 cm to 1.00 cm. These quantities were used to determine the TIN's models average relative and absolute errors.

Table 5. The results of measuring the sections, which are the main axes of the scale, drawn on the crackmeters in the direction: horizontal in the range from -2.00 mm to 2.00 mm and vertical: from -1.00 mm to 1.00 mm

Number of crackmeter	Horizontal length in range $<-2.00; 2.00>$ [cm]			Vertical length in range $<-1.00; 1.00>$ [cm]		
	Size on the TIN model [cm]	Absolute error [cm]	Relative error [%]	Size on the TIN model [cm]	Absolute error [cm]	Relative error [%]
S1	3.93	0.07	1.75	1.95	0.05	1.25
S2	3.86	0.14	3.50	1.91	0.09	2.25
S3	3.81	0.19	4.75	1.93	0.07	1.75
S4	3.85	0.15	3.75	1.90	0.10	2.50
S5	4.08	0.08	2.00	2.06	0.06	1.50
S6	3.86	0.14	3.50	1.93	0.07	1.75
S8	4.12	0.12	3.00	1.98	0.02	0.50
S9	4.01	0.01	0.25	2.01	0.01	0.25
S10	3.89	0.11	2.75	1.96	0.04	1.00
S11	3.99	0.01	0.25	1.99	0.01	0.25
S12	3.99	0.01	0.25	1.98	0.02	0.50
S13	4.06	0.06	1.50	2.03	0.03	0.75
S14	3.95	0.05	1.25	1.98	0.02	0.50
S15	3.95	0.05	1.25	1.95	0.05	1.25
S16	3.82	0.18	4.50	1.94	0.06	1.50
S17	4.08	0.08	2.00	2.01	0.01	0.25
S18	3.91	0.09	2.25	1.90	0.10	2.50
Average	3.95	0.09	2.26	1.97	0.05	1.19

Table 5 shows the results of measurements of the main axes of the pitch, which is on eighteen crackmeters. The average length of the horizontal section is 3.95 cm, with an average absolute error of 0.09 cm. The average length of the vertical section is 1.97 cm with an average absolute error of 0.05 cm. The average relative error of the horizontal section equals 2.26 %, while the average relative error of the vertical section is 1.19 %. The resulting measurement errors of the horizontal section are, on average, twice as large as the measurement errors of the vertical section. This conclusion is related to the fact that the nominal length of the horizontal section is twice that of the vertical section. Such a correlation may indicate a scale factor in point clouds and TIN grids. This confirms that the mapping error of objects using a smartphone with the Pix4Dcatch app increases proportionally to the increase in object size. Based on the calculated average errors, it is possible to conclude the method's usefulness for measuring the width of cracks. Despite the fact that the data is produced in the process of photogrammetric processing of images without tie points, it is possible to detect changes of 1 mm in size from the data.

The orthophotomap and front façade point cloud obtained from the UAV are in a global coordinate system, one for the entire palace. The orientation of the smartphone data is approximate. Each point cloud recorded from the smartphone is in a different local coordinate system. The tie points on the exterior façade of the Palace have a precise location in the global coordinate system.

On the other hand, there are no tie points on the interior walls of the Palace. Therefore, smartphone measurements cannot be realized in the global coordinate system. The network was not stabilized inside the palace due to conservation and lack of tachymetric measurements.

The location of individual cracks relative to the global layout of the site can be approximated. Data on the width of cracks at individual sections should be stored in databases. On the other hand, to determine the effect of the size of crack changes on the entire object, attention should be paid to the direction of the changes. The direction of cracks on walls is usually vertical. Over time, cracks on walls usually widen, that is, they increase their width in the plane of the wall. As the conducted research has shown, 2D and 3D photogrammetric data acquisition technology is suitable for recording such changes in walls. Based on the data acquired by UAV and smartphone, it is possible to accurately determine the

width of cracks ranging in size from several millimetres to tens of millimetres.

6 Discussion

Using unmanned aerial vehicles and mobile technologies allows a non-invasive inventory of historic buildings. As a result of image processing with specialized photogrammetric software, a point cloud is generated, based on which it is possible to determine the geometry and shape of objects, as well as the degree of their degradation. Each point of the cloud has specific coordinates in the spatial rectangular coordinate system. Each cloud point also has coordinates in the RGB colour space model, which facilitates identification of details and makes point cloud classification more accurate.

It should be noted that the structural health of the building, i.e., the degree of deterioration and damage to the walls, is also monitored by traditional methods. As part of the ongoing research, periodic readings are also captured from sensors stabilized in the Mieroszewski Palace. The readings of crack gauges installed near the largest cracks are recorded. At six-month intervals, data are also read from the specific inclinometer, which has been operating on the second floor, as well as from an ultrasonic inclinometer operating in the attic. Moreover, precise levelling has been performed to determine the height differences of control benchmarks placed on the palace walls and its surroundings. Data collection from crackmeters and inclinometers provides accurate information on the progress of the site's structural changes. The data also provides a reference point for testing remote technologies for recording the surfaces. The research described is part of a major project integrating data from various sources. It is planned to develop the concept of modelling all measurements taken at the Palace. It was necessary to determine the accuracy of the data acquired using a UAV and a smartphone, before comparing it with the data from other sensors: an ultrasonic inclinometer, a laser scanner or precise levelling.

To determine the correlation between the magnitude of crack changes and other sensors' data, it is necessary to orient all readings related to the same coordinate system. Such a location does not have to be precise; hence, it can be approximated. The most important thing is to determine the directions of ongoing changes, for example, to determine the axes' coherence with the reference frame.

Partial models are assigned approximate coordinates in a globally unified system for the entire Palace in the concept described. Due to the vertical cracks appearing on the palace walls, monitoring the changes encompasses periodic measurements of the width of these cracks along the walls and, therefore, in the horizontal direction. The presented study showed that the analyzed technologies for remote object inventory are helpful and sufficiently accurate for such measurements.

Research shows that the proposed methodology for determining crack widths is accurate enough to detect changes of 1 mm in size. It is an undoubted advantage. Besides, the object registration time is relatively short, and measuring equipment is currently readily available. The only difficulty in obtaining accurate data is proper processing. The products of photogrammetric processing of images, i.e., point clouds, mesh grids, or true ortho, are subject to a high probability of distortion in the form of overscaling the presence of a scale factor in the survey material. The most significant error is in the depth of the images. This is the primary disadvantage of close-range photogrammetry.

On the other hand, as studies have confirmed, coordinates with higher accuracy are obtained in the plane of the images. It is this property that was used to determine the width of the cracks. The theoretical basis for estimating measurement error is the subject of many literature positions – e.g., [Piotrowski and Kostyrko \(2012\)](#); [Taylor \(1999\)](#).

7 Conclusions

The details of spatial data acquired using non-invasive geoinformation technologies are satisfactory for assessing the degree of degradation and deterioration of historic buildings. The accuracy of spatial data generated by photogrammetric image matching is sufficient to detect more than 1 mm changes. Studies on the feasibility of using images from the DJI Mavic 3 Enterprise RTK showed an average accuracy of 1 mm for measuring the width of cracks. The metricity of these data depends on the direction and distance of the segment between two points relative to the vertical façade plane.

The research on measuring the width of cracks and fissures using a Samsung Galaxy S20 FE smartphone showed an average absolute error of 0.24 mm and an average relative error of 3.34%. The high accuracy of the spatial data, especially in the façade surface, results in a high probability of accurately determining the width of cracks and fissures. On the walls and vertical elements of the structure, the direction of these changes is vertical (they run from top to bottom). Given such peculiarities of the structure, measuring the width of cracks and checking the rate of their changes in the horizontal plane plays a vital role in wall monitoring.

In the project's next stage, the authors plan to use the research described in the article to model the changes in the Palace. They plan to compare the results of periodic measurements and develop a procedure for automatically detecting changes in crack widths.

Acknowledgements

The presented material is part of the research conducted under the grants of the Scientific Council of the Discipline of Civil Engineering, Geodesy, and Transport, Warsaw University of Technology, titled "Evaluation and modelling of geometric changes in the structures of historical buildings located in endangered areas" (Karsznia K.) and "Application of modern 3D modelling tools to determine the technical condition of historic buildings" (Świerczyńska E.).

All works were carried out in collaboration between the Warsaw University of Technology and the Museum of the Coal Basin Area in Będzin, Poland.

The authors also want to thank Mr. Piotr Rozenbajgier from NaviGate Sp. z o.o. for his significant contribution to the paper by providing UAV flights and data processing.

References

- Baca, M., Muszyński, Z., Rybak, J., and Żyrek, T. (2015). The application of geodetic methods for displacement control in the self-balanced pile capacity testing instrument. In *Advances and trends in engineering sciences and technologies: proceedings of the International Conference on Engineering Sciences and Technologies, Tatrská Štrba, Slovakia*, pages 15–20.
- Baltsavias, E. P. (1999). A comparison between photogrammetry and laser scanning. *ISPRS Journal of Photogrammetry and Remote Sensing*, 54(2–3):83–94, doi:10.1016/S0924-2716(99)00014-3.
- Baselga, S., Garrigues, P., Berné, J. L., Anquela, A. B., and Martín, A. (2011). Deformation monitoring in historic buildings: A case study. *Survey Review*, 43(323):484–492, doi:10.1179/003962611X13117748891912.
- Bolognesi, M., Furini, A., Russo, V., Pellegrinelli, A., and Russo, P. (2014). Accuracy of cultural heritage 3D models by RPAS and terrestrial photogrammetry. *The International Archives of the Photogrammetry, Remote Sensing and Spatial Information Sciences*, XL-5:113–119, doi:10.5194/isprsarchives-xl-5-113-2014.
- Buill, F., Núñez-Andrés, M. A., Costa-Jover, A., Moreno, D., Puche, J. M., and Macias, J. M. (2020). Terrestrial Laser Scanner for the formal assessment of a Roman–Medieval structure – The cloister of the cathedral of Tarragona (Spain). *Geosciences*, 10(11):427, doi:10.3390/geosciences10110427.
- Błaszczak-Bąk, W., Suchocki, C., Kozakiewicz, T., and Janicka, J. (2023). Measurement methodology for surface defects inventory of building wall using smartphone with light detection and ranging sensor. *Measurement*, 219:113286, doi:10.1016/j.measurement.2023.113286.
- Chen, M.-C., Wang, K., and Xie, L. (2013). Deterioration mechanism of cementitious materials under acid rain attack. *Engineering Failure Analysis*, 27:272–285, doi:10.1016/j.engfailanal.2012.08.007.
- Corradetti, A., Seers, T., Billi, A., and Tavani, S. (2021). Virtual outcrops in a pocket: The smartphone as a fully equipped photogrammetric data acquisition tool. *GSA Today*, 31(9):4–9, doi:10.1130/gsatg506a.1.
- Di Stefano, F., Cabrelles, M., García-Asenjo, L., Lerma, J. L., Malinverni, E. S., Baselga, S., Garrigues, P., and Pierdicca, R. (2020). Evaluation of long-range mobile mapping system (MMS) and close-range photogrammetry for deformation monitoring. A case study of Cortes de Pallás in Valencia (Spain). *Applied Sciences*, 10(19):6831, doi:10.3390/app10196831.
- Fawzy, H. E.-D. (2019). Study the accuracy of digital close range photogrammetry technique software as a measuring tool. *Alexandria Engineering Journal*, 58(1):171–179, doi:10.1016/j.aej.2018.04.004.
- Gairns, C. (2008). Development of a semi-automated system for structural deformation monitoring using a reflectorless total station. Master's thesis, Department of Geodesy and Geomatics Engineering, University of New Brunswick, Fredericton, Canada.
- Gollob, C., Ritter, T., Kraßnitzer, R., Tockner, A., and Nothdurft, A. (2021). Measurement of forest inventory parameters with Apple iPad Pro and integrated LiDAR technology. *Remote Sensing*, 13(16):3129, doi:10.3390/rs13163129.
- Jaud, M., Kervot, M., Delacourt, C., and Bertin, S. (2019). Potential of smartphone SfM photogrammetry to measure coastal morphodynamics. *Remote Sensing*, 11(19):2242, doi:10.3390/rs11192242.
- Jigyasu, R. (2005). Towards developing methodology for integrated risk management of cultural heritage sites and their settings. In *15th ICOMOS General Assembly and International Symposium: "Monuments and sites in their setting – conserving cultural heritage in changing townscapes and landscapes"*, 17–21.10.2005, Xi'an, China.
- Karsznia, K. (2023). Innowacyjny system geomonitoringu do bada-

- nia deformacji elementów powierzchniowych – IMS GEO (Innovative geomonitoring system for studying surface element deformations – IMS GEO). *PRZEGLĄD GEODEZYJNY*, 1(8):22–26, doi:10.15199/50.2023.08.3.
- Karsznia, K. (2024). Wykorzystanie wieloźródłowych danych przestrzennych do oceny stanu obiektów zabytkowych na terenach zagrożonych (using multi-source spatial data to assess the condition of historic buildings in endangered areas). *PRZEGLĄD GEODEZYJNY*, 1(2):38–42, doi:10.15199/50.2024.2.5.
- Lohani, B. and Ghosh, S. (2017). Airborne lidar technology: A review of data collection and processing systems. *Proceedings of the National Academy of Sciences, India Section A: Physical Sciences*, 87(4):567–579, doi:10.1007/s40010-017-0435-9.
- Markiewicz, J., Tobiasz, A., Kot, P., Muradov, M., Shaw, A., and Al-Shammaa, A. (2019). Review of surveying devices for structural health monitoring of cultural heritage buildings. In *2019 12th International Conference on Developments in eSystems Engineering (DeSE)*. IEEE, doi:10.1109/dese.2019.00113.
- Murtiyoso, A. and Grussenmeyer, P. (2017). Documentation of heritage buildings using close-range UAV images: dense matching issues, comparison and case studies. *The Photogrammetric Record*, 32(159):206–229, doi:10.1111/phor.12197.
- Museum of the Coal Basin (2024). Museum of the Coal Basin in Będzin. <https://www.muzeumzaglebia.pl>.
- Ornoch, L., Popielski, P., Olszewski, A., and Kasprzak, A. (2021). Ultrasonic sensors enabling early detection of emergency trends and analysis of structure inclination and stability by means of highly accurate level measurements. *Sensors*, 21(5):1789, doi:10.3390/s21051789.
- Pearson, K. (1896). VII. Mathematical contributions to the theory of evolution – III. Regression, heredity, and panmixia. *Philosophical Transactions of the Royal Society of London. Series A, containing papers of a mathematical or physical character*, (187):253–318.
- PGI (2024). Polish Geological Institute. <https://geologia.pgi.gov.pl/arcgis>.
- Piotrowski, J. and Kostyrko, K. (2012). *Wzorcowanie aparatury pomiarowej (Calibration of measuring equipment)*. Wydawnictwo Naukowe PWN, Warszawa.
- Pix4D (2023). How can you know whether to use a drone or a terrestrial rover – the viDoc? One team compared the results of both to test the accuracy. <https://www.pix4d.com/blog/comparing-vidoc-rtk-rover-p1-camera>.
- Press, W. H., Teukolsky, S. A., Vetterling, W. T., and Flannery, B. P. (1992). *Numerical recipes in C*. Cambridge university press New York, NY.
- Sapirstein, P. (2016). Accurate measurement with photogrammetry at large sites. *Journal of Archaeological Science*, 66:137–145, doi:10.1016/j.jas.2016.01.002.
- Shevchenko, G. G., Bryn, M. J., Afonin, D. A., and Gura, D. A. (2020). *Experimental Researches in Defining Deformations by Free Station Method and Results Processing by Search Method*, pages 163–175. Springer Singapore, doi:10.1007/978-981-15-0454-9_17.
- Stec, K. (2007). Seismic hazard state in the Upper Silesian Coal Basin. *Research Reports Mining and Environment, Quarterly*, (3):55–75.
- Świerczyńska, E., Karsznia, K., Książek, K., Odziemczyk, W., and Smaczyński, M. (2023). Assessing the technical state of historical buildings using Terrestrial Laser Scanning and close-range aerial photogrammetry. In *XVI International Scientific and Technical Conference entitled "Current Problems in Engineering Geodesy – Engineering Geodesy for the Development of a Sustainable Economy"*, Poznań-Baranowo, 21–23.09.2023.
- Taylor, J. R. (1999). Wstęp do analizy błędów pomiarowego (Introduction to measurement error analysis).
- Teppati Losè, L., Spreafico, A., Chiabrandò, F., and Giulio Tonolo, F. (2022). Apple LiDAR sensor for 3D surveying: Tests and results in the cultural heritage domain. *Remote Sensing*, 14(17):4157, doi:10.3390/rs14174157.
- Woźniak, M. (2009). Bezreflektorowe systemy pomiarowe w monitorowaniu przemieszczeń (Reflectorless measurement systems for displacement monitoring). Technical Report 443, Instytut Techniki Budowlanej. Bezdotykowe metody obserwacji i pomiarów obiektów budowlanych. Instrukcje, wytyczne, poradniki.
- Woźniak, M. and Woźniak, K. (2020). MarQR technology for measuring relative displacements of building structure elements with regard to joints and cracks. *Reports on Geodesy and Geoinformatics*, 109(1):33–40, doi:10.2478/rgg-2020-0005.
- Woźniak, M., Świerczyńska, E., and Jastrzębski, S. (2015). The use of video-tacheometric technology for documenting and analysing geometric features of objects. *Reports on Geodesy and Geoinformatics*, 99(1):28–43, doi:10.2478/rgg-2015-0010.
- Xie, S., Qi, L., and Zhou, D. (2004). Investigation of the effects of acid rain on the deterioration of cement concrete using accelerated tests established in laboratory. *Atmospheric Environment*, 38(27):4457–4466, doi:10.1016/j.atmosenv.2004.05.017.
- Zaczek-Peplinska, J. (2023). Pomiarzy inwentaryzacyjne z wykorzystaniem apple iphone 13 pro i zintegrowanej technologii lidar (Inventory measurements using Apple iPhone 13 Pro and integrated LiDAR technology). *PRZEGLĄD GEODEZYJNY*, 1(2):16–19, doi:10.15199/50.2023.02.1.